ADVANCED FUNCTIONAL MATERIALS

Supporting Information

for *Adv. Funct. Mater.*, DOI 10.1002/adfm.202307605

Molecular Auxetic Polymer of Intrinsic Microporosity via Conformational Switching of a Cavitand Crosslinker

*Francesca Portone, Mattia Amorini, Matteo Montanari, Roberta Pinalli, Alessandro Pedrini, Roberto Verucchi, Roberto Brighenti and Enrico Dalcanale**

Supporting Information

Molecular auxetic polymer of intrinsic microporosity via conformational switching of a cavitand crosslinker

*Francesca Portone, Mattia Amorini, Matteo Montanari, Roberta Pinalli, Alessandro Pedrini, Roberto Verucchi, Roberto Brighenti, Enrico Dalcanale**

CONTENTS

1. Experimental procedures

All commercial reagents, chemicals and solvents were purchased from Sigma Aldrich, TCI Chemical Europe and used as received. PIM1 was synthetized according to the reported procedure in literature.[1]

1.1. Synthesis of Qx2

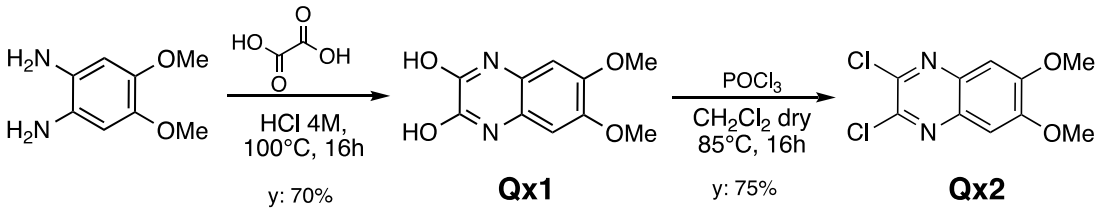

Scheme S1. Synthesis of 2,3-dichloro-6,7-dimethoxyquinoxaline (**Qx2**).

1.1.1. Synthesis of 6,7-dimethoxyquinoxaline-2,3-dione (**Qx1**)

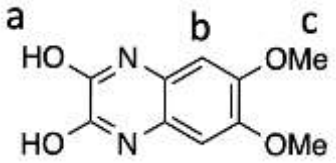

2-diamino-4,5-dimethoxy benzene (2 g, 10 mmol) was dispersed in HCl 4M (15 mL) and the suspension added to a solution of oxalic acid (1 g, 10 mmol) in HCl 4M (15 mL). The reaction mixture was heated at 100°C for 16 h. The formed precipitated was filtered and washed several times with water. The final product was obtained as dark purple solid. Yield: 1.81 g, 70%.

^{1}H NMR (400 MHz, DMSO-d_6) δ (ppm): 11.73 (s, 2H, H_a), 6.73 (s, 2H, H_b), 3.73 (s, 6H, H_c).

^{13}C NMR (101 MHz, DMSO-d_6) δ (ppm): 155.36, 140.90, 116.23, 105.36, 56.85.

GC-MS: m/z 223.40 $[M+H]^+$.

*1.1.2. Synthesis of 2,3-dichloro-6,7-dimethoxyquinoxaline (***Qx2***)*

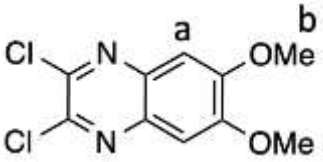

To a solution of 6,7-dimethoxyquinoxaline-2,3-dione (1 g, 4.5 mmol) in 40 mL of dry CH_2Cl_2 (40 mL), $POCl_3$ (1.71 mL, 18 mmol) and three drops of DMF were added. The reaction mixture was stirred at 85°C for 16 h. Afterwards, the solvent was removed under vacuum and the obtained solid was dissolved in CH_2Cl_2 (DCM) and filtered through celite. The final product was purified by flash column chromatography on silica gel in DCM giving a white powder. Yield: 750 mg, 75%.

^{1}H NMR (400 MHz, $CDCl_3$) δ (ppm): 7.31 (s, 2H, H_a), 4.06 (s, 6H, H_b).

^{13}C NMR (101 MHz, $CDCl_3$) δ (ppm): 153.72, 137.91, 105.70, 56.53.

GC-MS: m/z 260.1 $[M+H]^+$.

1.2. Synthesis of cavitand C_V8H

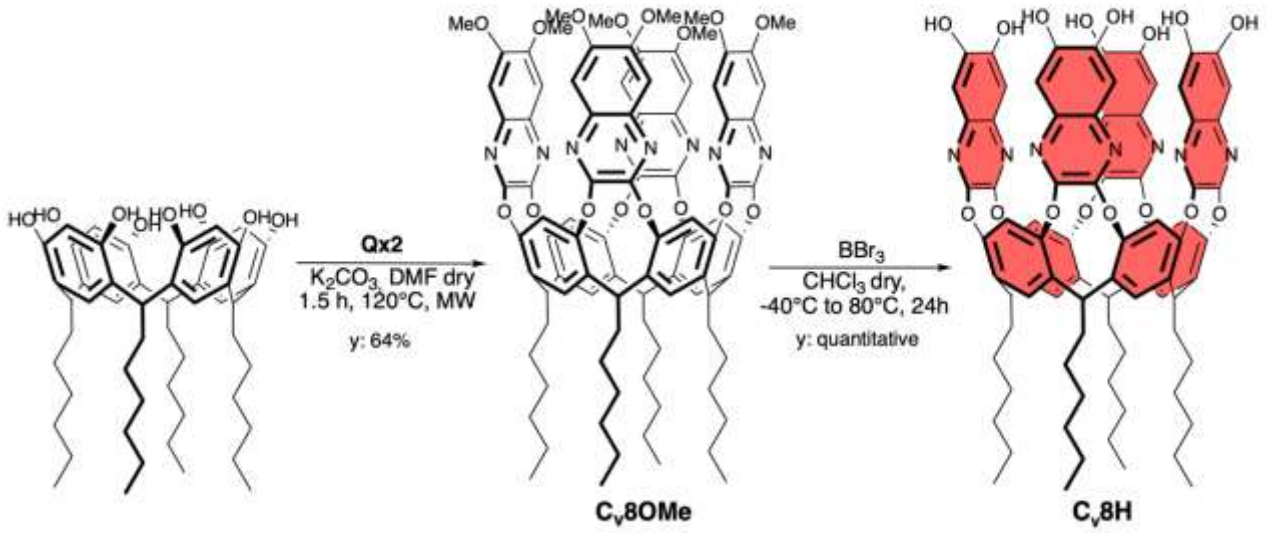

Scheme S2. Synthesis of cavitand **C_V8H**.

1.2.1. Synthesis of cavitand C_V8OMe

In a microwave reactor, under dry condition, **Res[C_6H_{13},H]** (168 mg, 0.20 mmol), anhydrous potassium carbonate (280 mg, 2.0 mmol) and **Qx2** (232 mg, 0.90 mmol) were dissolved in dry DMF (9 mL). The mixture was heated at 120°C for 1.5 h (200 W). Subsequently, the solvent was removed under reduced pressure and the crude product was then purified by flash column chromatography on silica gel (DCM/EtOAc 100/0 → 95:5). The final product was obtained as pale-yellow solid. Yield: 205 mg, 64%.

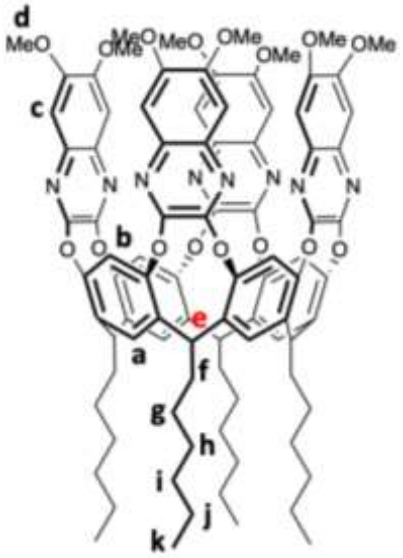

^{1}H NMR (400 MHz, $CDCl_3$) δ (ppm): 7.59 (s, 4H, H_a), 7.23 (s, 8H, H_c), 7.01 (s, 4H, H_b), 4.56 (m, 4H, H_e), 3.98 (s, 24H, H_d), 2.13 (m, 8H, H_f), 1.29 (m, 32H, $H_{g\text{-}j}$), 0.88 (t, 12H, J = 8Hz, H_k).

^{13}C NMR (101 MHz, $CDCl_3$) δ (ppm): 152.86, 152.14, 150.61, 148.52, 135.83, 133.66, 123.82, 106.21, 56.34, 36.04, 32.23, 31.81, 29.29, 27.49, 22.75, 14.15.

MALDI-TOF: calculated for $C_{92}H_{96}N_8O_{16}$ $[M + H]^+$ m/z: 1569.70, found m/z: 1569.51.

1.2.2. Synthesis of cavitand ***C_V8H***

C_V8OMe (110 mg, 0.07 mmol) was dissolved in dry chloroform (20 mL) and cooled in acetone/liquid nitrogen bath at -40°C. BBr_3 1M in CH_2Cl_2 (8.4 mL, 8.4 mmol) was added dropwise. The mixture was stirred for 24 h at 80°C. After cooling to room temperature, the rection was quenched with water and some drops of HCl 1M. The residual chloroform was removed under vacuum and the yellow precipitate was filtered and dried under vacuum to obtain the final product in quantitative yield.

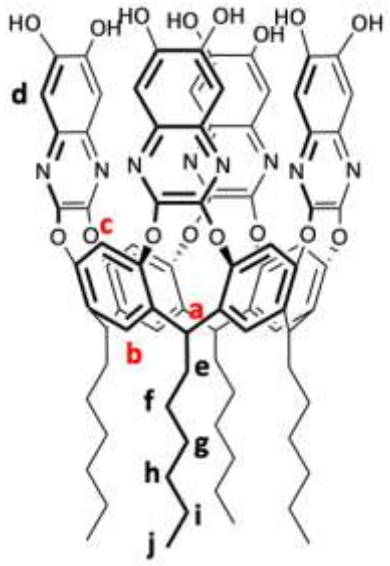

^{1}H NMR (400 MHz, acetone-d_6) δ (ppm): 8.14 (s, 4H, H_c), 7.82 (s, 4H, H_b), 7.27 (s, 8H, H_d), 5.70 (t, 4H, H_a), 2.42 (q, 8H, H_e), 1.33 (m, 32H, $H_{f\text{-}i}$), 0.94 (t, 12H, J = 8Hz, H_j).

^{13}C NMR (101 MHz, acetone-d_6) δ (ppm): 152.79, 150.14, 149.13, 136.07, 124.60, 118.52, 109.25, 34.23, 31.98, 31.85, 28.07, 22.48, 13.48.

HR-ESI-MS: calculated for $C_{92}H_{96}N_8O_{16}$ $[M + H]^+$ m/z: 1457.58151, found m/z: 1457.58523.

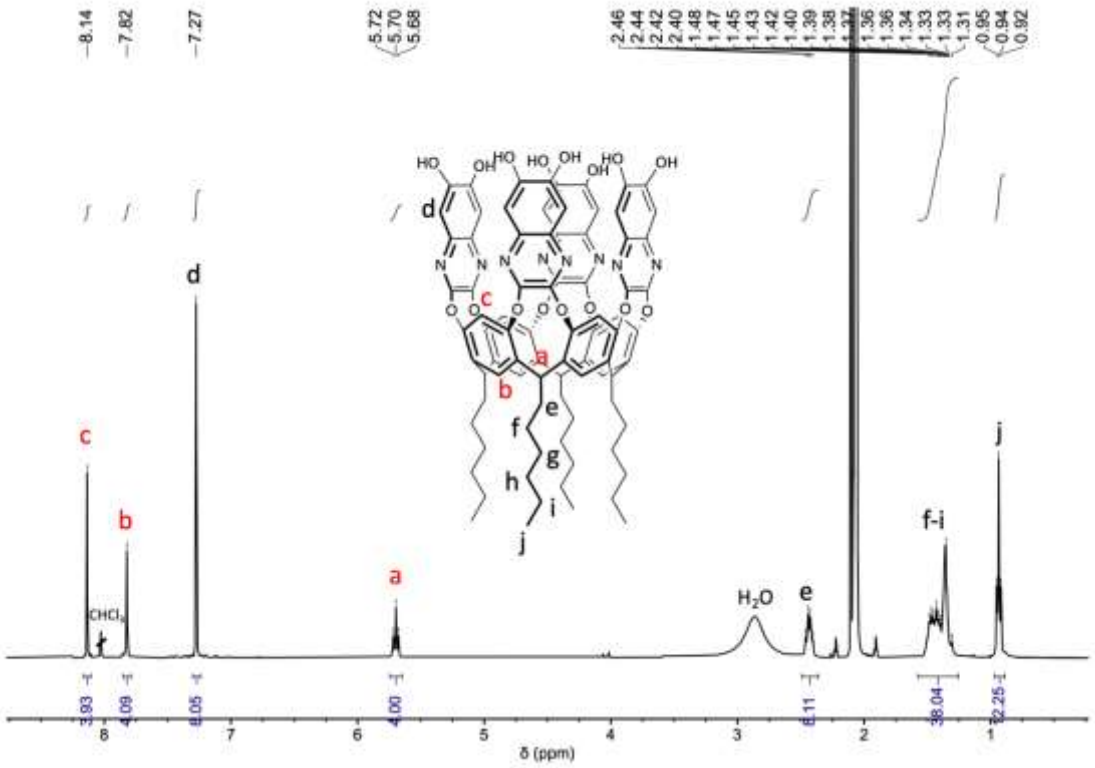

Figure S1. ^{1}H NMR spectrum of **C_V8H** (acetone-d_6, 400 MHz, 25°C).

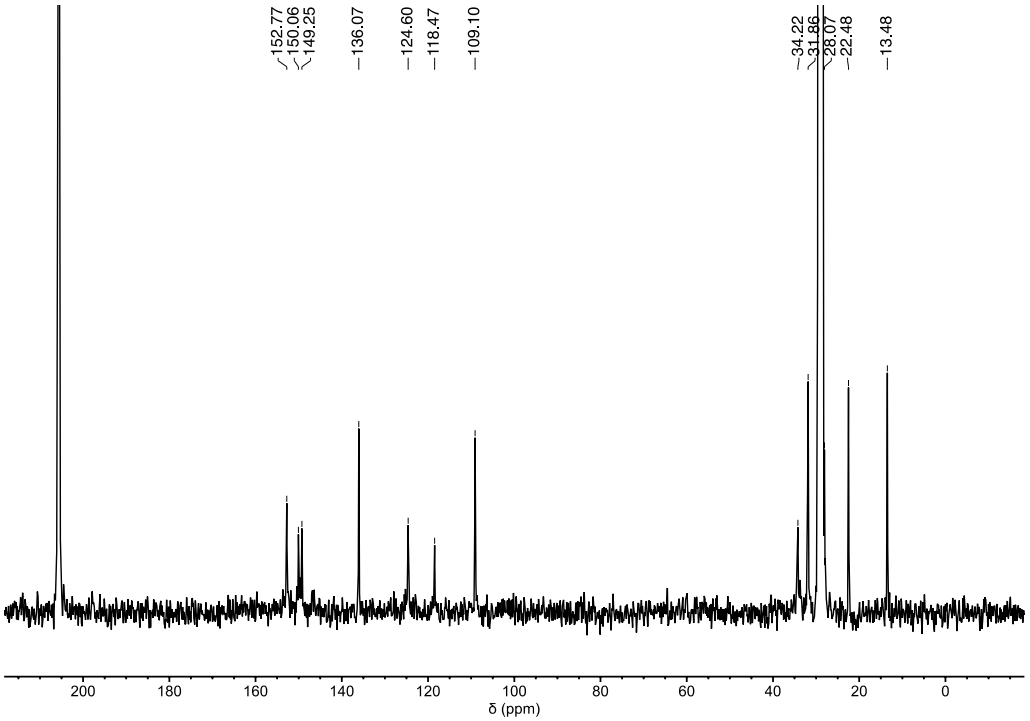

Figure S2. ^{13}C NMR spectrum of **C_V8H** (acetone-d_6, 101 MHz, 25°C).

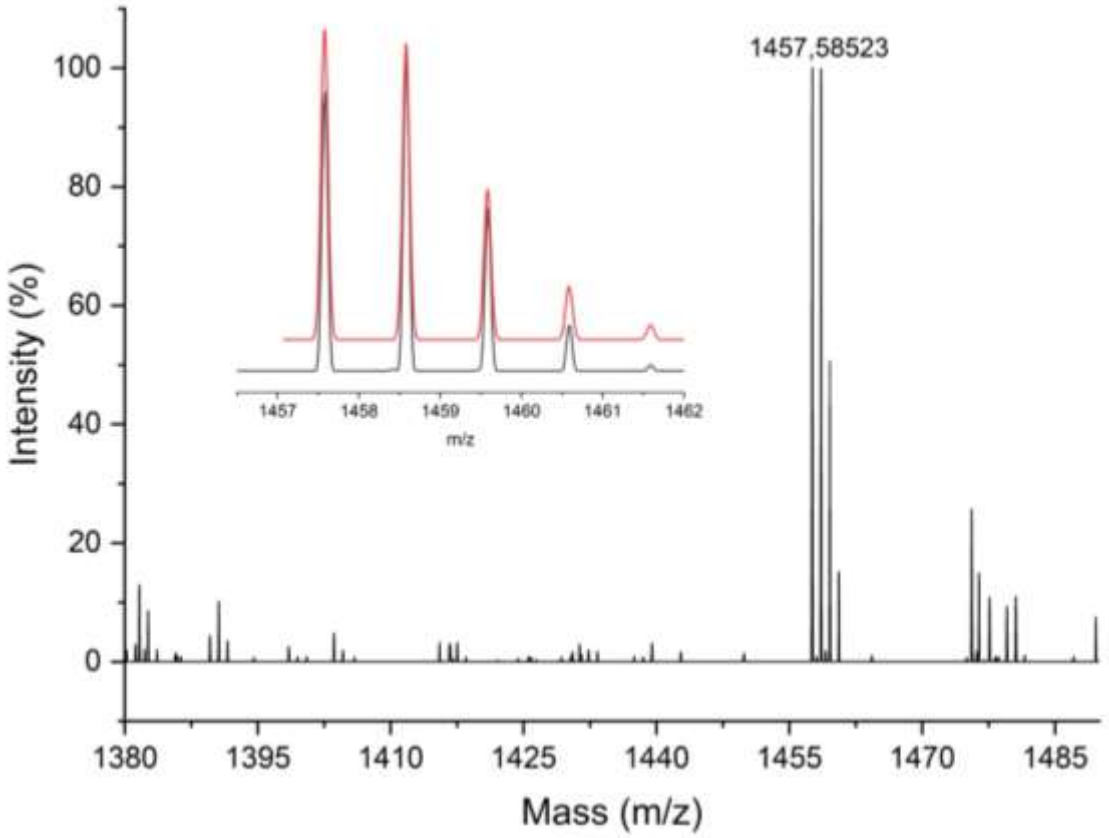

Figure S3. HR-ESI-MS spectrum of **C_V8H** with experimental (black line) versus theoretical (red line) isotopic distribution in the inset.

1.3. Synthesis of cavitand C_K8H

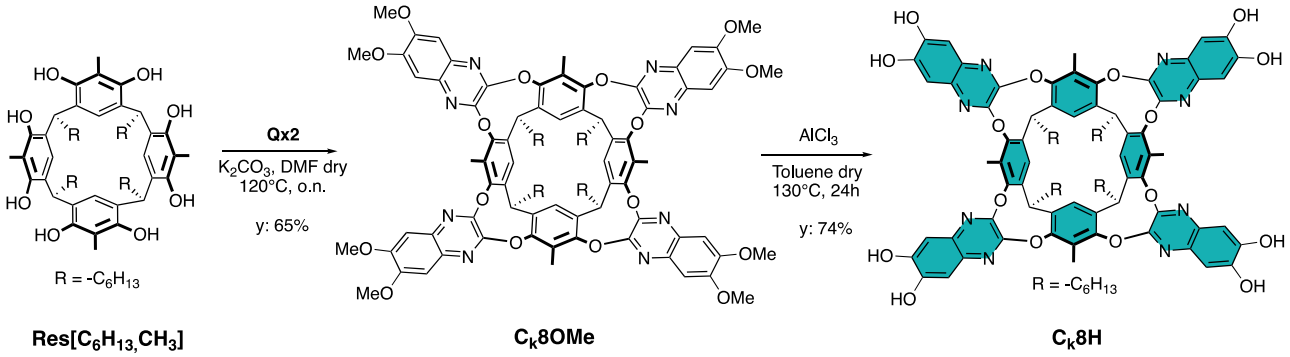

Scheme S3. Synthesis of cavitand **C_K8H**.

1.3.1. Synthesis of cavitand C_K8OMe

Res[C_6H_{13}, CH_3] (100 mg, 0.11 mmol), anhydrous potassium carbonate (157 mg, 1.13 mmol) and **Qx2** (129 mg, 0.50 mmol) were added in dry DMF (4mL) and reacted at 120°C for 16 h. The reaction mixture was then precipitated in HCl 1M and the collected filtrate was purified by column chromatography on silica gel (DCM/EtOAc 9/1 → 7/3). The final product was obtained as yellow solid. Yield: 120 mg, 65%.

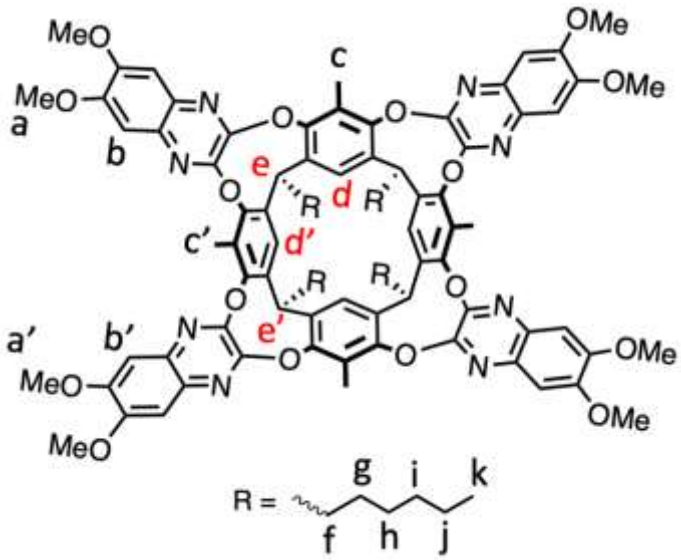

^{1}H NMR (400 MHz, $CDCl_3$) δ (ppm): 7.00 (s, 4H, H_b), 6.87 (s, 2H, H_d), 6.58 (s, 4H, $H_{b'}$), 6.15 (s, 2H, $H_{d'}$), 4.17 (s, 12H, H_a), 3.95 (s, 12H, $H_{a'}$), 3.68-3.64 (m, 4H, $H_{d\text{-}d'}$), 3.08 (s, 6H, H_c), 2.26 (s, 6H, $H_{c'}$), 1.86 (m, 8H, H_f), 1.13-1.10 (m, 32H, $H_{g\text{-}j}$), 0.73 (t, 12H, J = 8Hz, H_k).

^{13}C NMR (101 MHz, $CDCl_3$) δ (ppm): 152.70, 151.39, 150.65, 150.31, 148.17, 144.37, 134.57, 133.96, 133.23, 129.94, 128.66, 122.54, 117.57, 117.20, 106.23, 105.22, 56.38, 55.92, 37.54, 32.25, 31.50, 29.71, 29.24, 27.11, 22.51, 13.90, 12.16, 11.30, 1.03.

MALDI-TOF: calculated for $C_{96}H_{104}N_8O_{16}$ $[M + H]^+$ m/z: 1625.76, found m/z: 1625.60.

1.3.2. Synthesis of cavitand ***C_K8H***

Under dry conditions, $AlCl_3$ (110 mg, 0.86 mmol) was added to a solution of **C_K8OMe** (70 mg, 0.043 mmol) in dry toluene (4 mL), and the mixture reacted at 130°C for 24 h. The reaction was then quenched in HCl 1M and the precipitate was filtered and washed several times with water. The product was further purified by dissolving in methanol and precipitating in hexane. Yield: 48 mg, 74%.

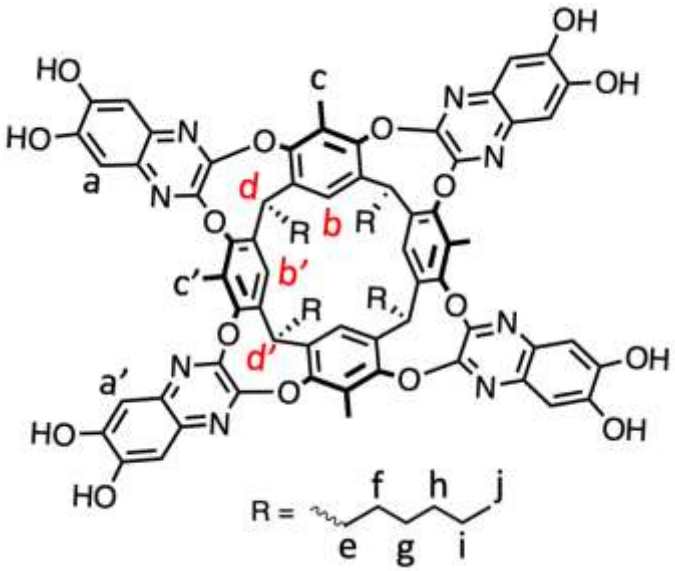

^{1}H NMR (400 MHz, CD_3OD) δ (ppm): 7.04 (s, 4H, H_a), 6.92 (s, 2H, H_b), 6.57 (s, 4H, $H_{a'}$), 6.24 (s, 2H, $H_{b'}$), 3.61-3.59 (m, 4H, $H_{d-d'}$), 3.09 (s, 6H, H_c), 2.14 (s, 6H, $H_{c'}$), 1.96-1-86 (m, 8H, H_e), 1.15-1.09 (m, 32H, H_{f-i}), 0.75 (t, 12H, J = 8Hz, H_i).

^{13}C NMR (101 MHz, CD_3OD) δ (ppm): 152.79, 150.48, 149.45, 148.55, 147.47, 143.86, 133.76, 133.38, 129.80, 118.20, 117.67, 108.82, 107.21, 37.25, 33.85, 31.63, 31.43, 29.35, 29.07, 28.63, 28.54, 28.13, 26.74, 22.34, 22.17, 18.51, 13.05, 12.95, 12.25, 11.47.

HR-ESI-MS: calculated for $C_{88}H_{88}N_8O_{16}$ $[M + H]^+$ m/z: 1513.63911, found m/z: 1513.64845, calculated for $[2M + 2H]^{2+}$ m/z: 1513.63911, found m/z: 1513.64845.

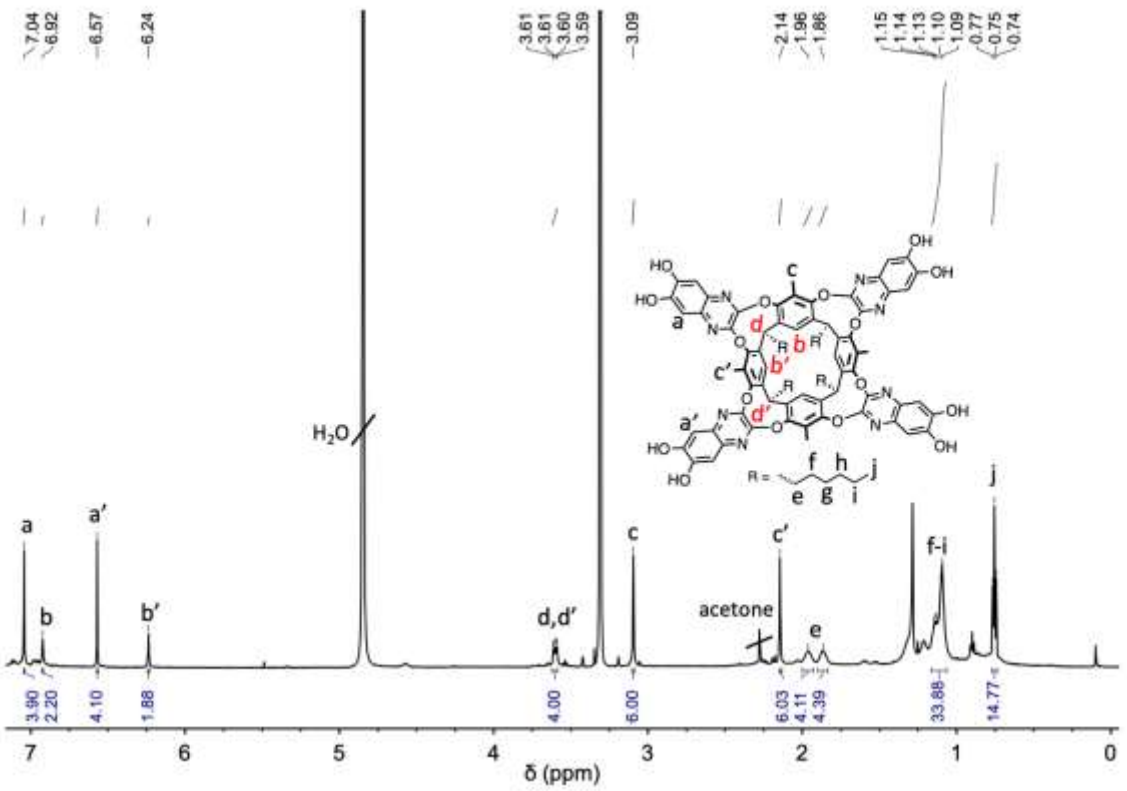

Figure S4. ^{1}H NMR spectrum of $\mathbf{C_K8H}$ (CD_3OD, 400 MHz, 25°C).

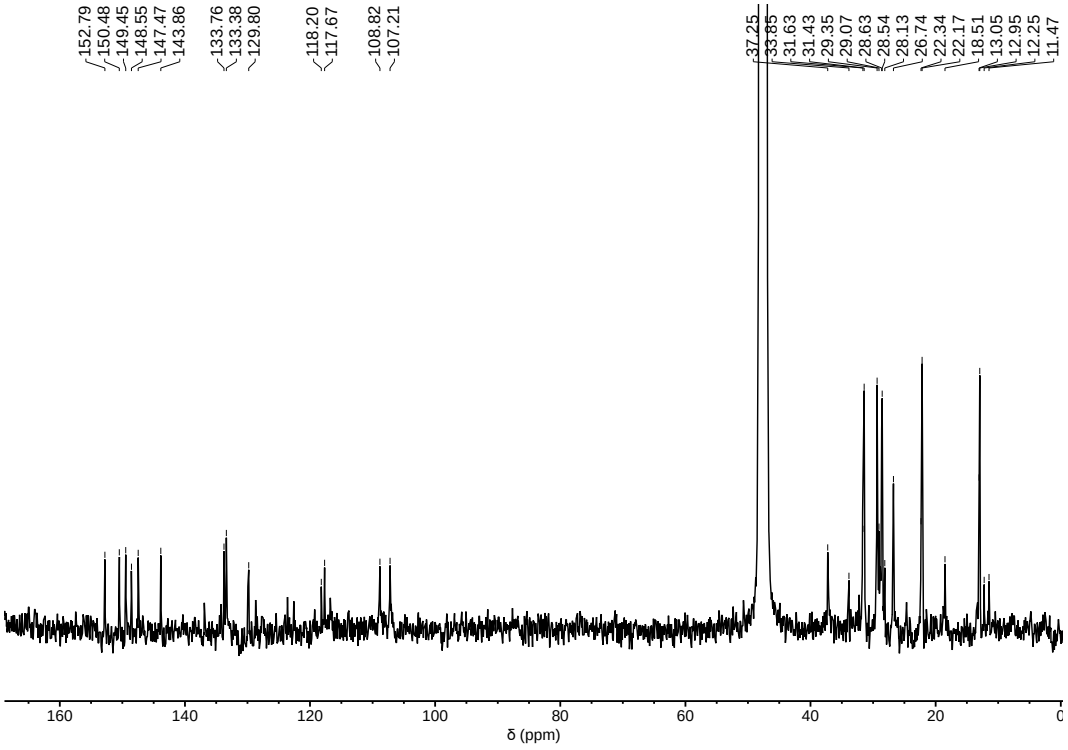

Figure S5. ^{13}C NMR spectrum of $\mathbf{C_K8H}$ (CD_3OD, 101 MHz, 25°C).

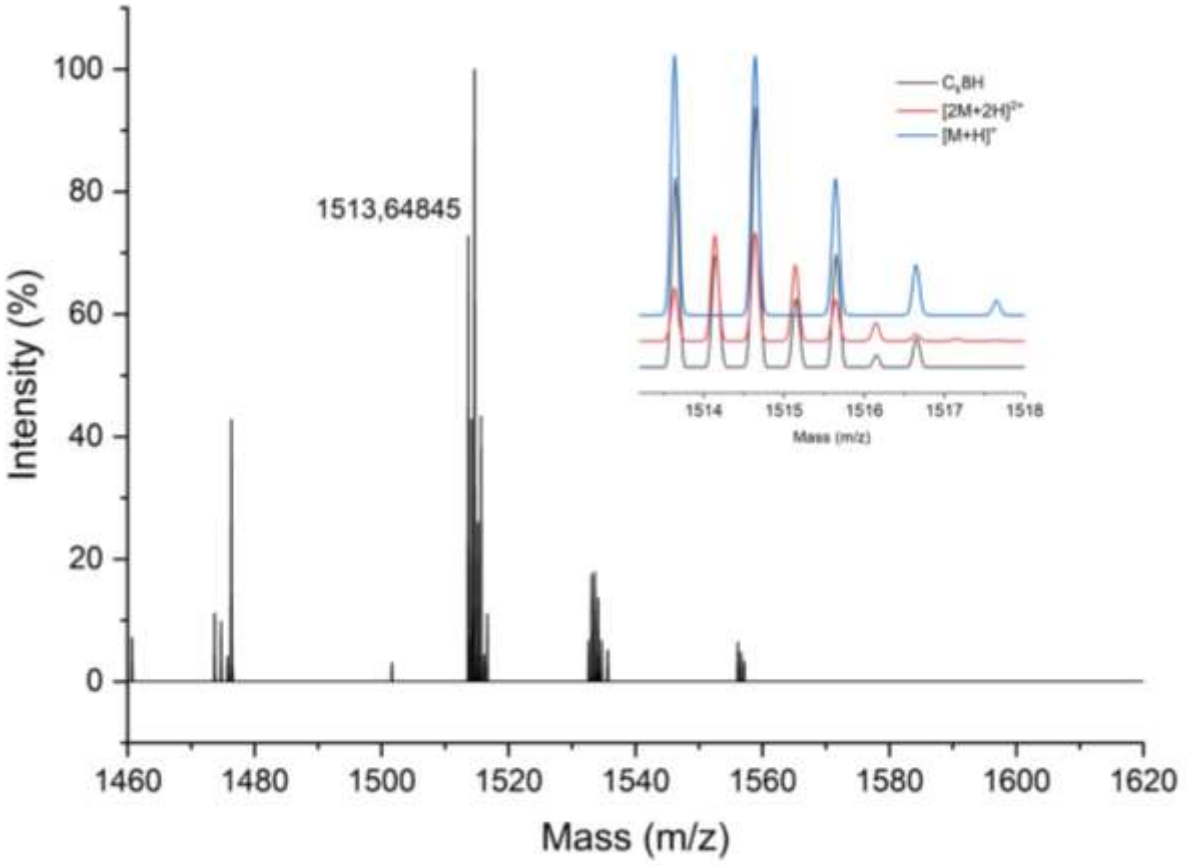

Figure S6. HR-ESI-MS spectrum of **C_K8H** with experimental (black line) versus theoretical (red and blue line) isotopic distributions in the inset.

1.4. Synthesis of the crosslinked PIM1-C_V8H

TTSBI (470 mg, 1.38 mmol, 0.92 eq) and **C_V8H** (88 mg, 60 μmol, 0.04 eq) were dissolved in dry DMF (45 mL). Anhydrous potassium carbonate (932 mg, 6.75 mmol) was added to the solution and the mixture was kept stirring at room temperature for 15 minutes, followed by the addition of **TFTPN** (300 g, 1.5 mmol, 1 eq). The reaction was stirred at 60 °C for 3 days, observing the formation of a yellow precipitate. The mixture was quenched in water (300 mL), allowing the precipitation of the polymer that was filtered and washed several times with water and methanol. The product was further purified by refluxing in water (300 mL) for 4 hours, and 0.722 g of the product were recovered as yellow powder after filtration and drying in a vacuum oven at 60 °C for 2 days.

The procedure described above was adopted for the synthesis of **PIM1-C_K8H** (**Scheme S4**), replacing **C_V8H** with **C_K8H,** using the same equivalents of the components.

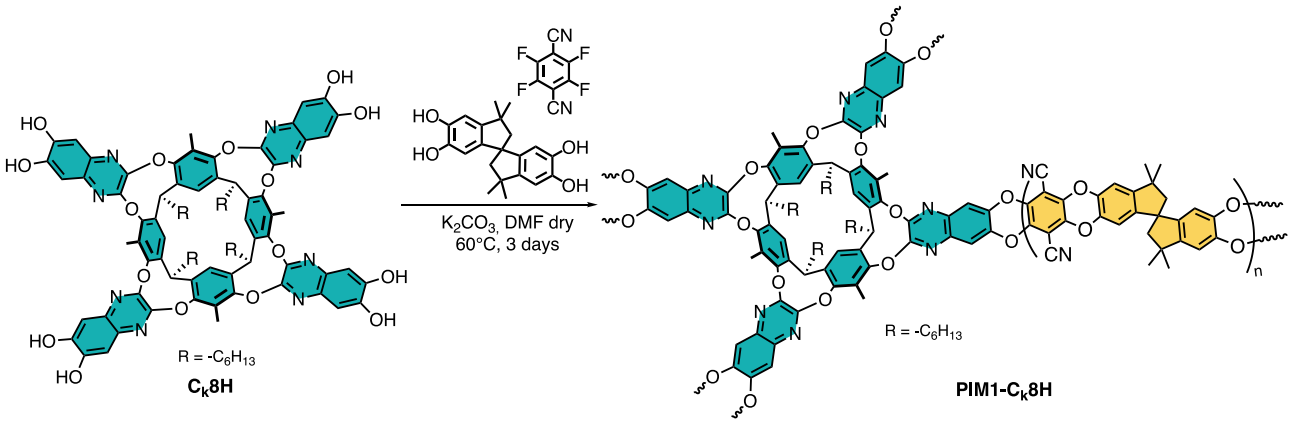

Scheme S4. Synthesis of **PIM1-C$_k$8H**.

2. IR Spectra

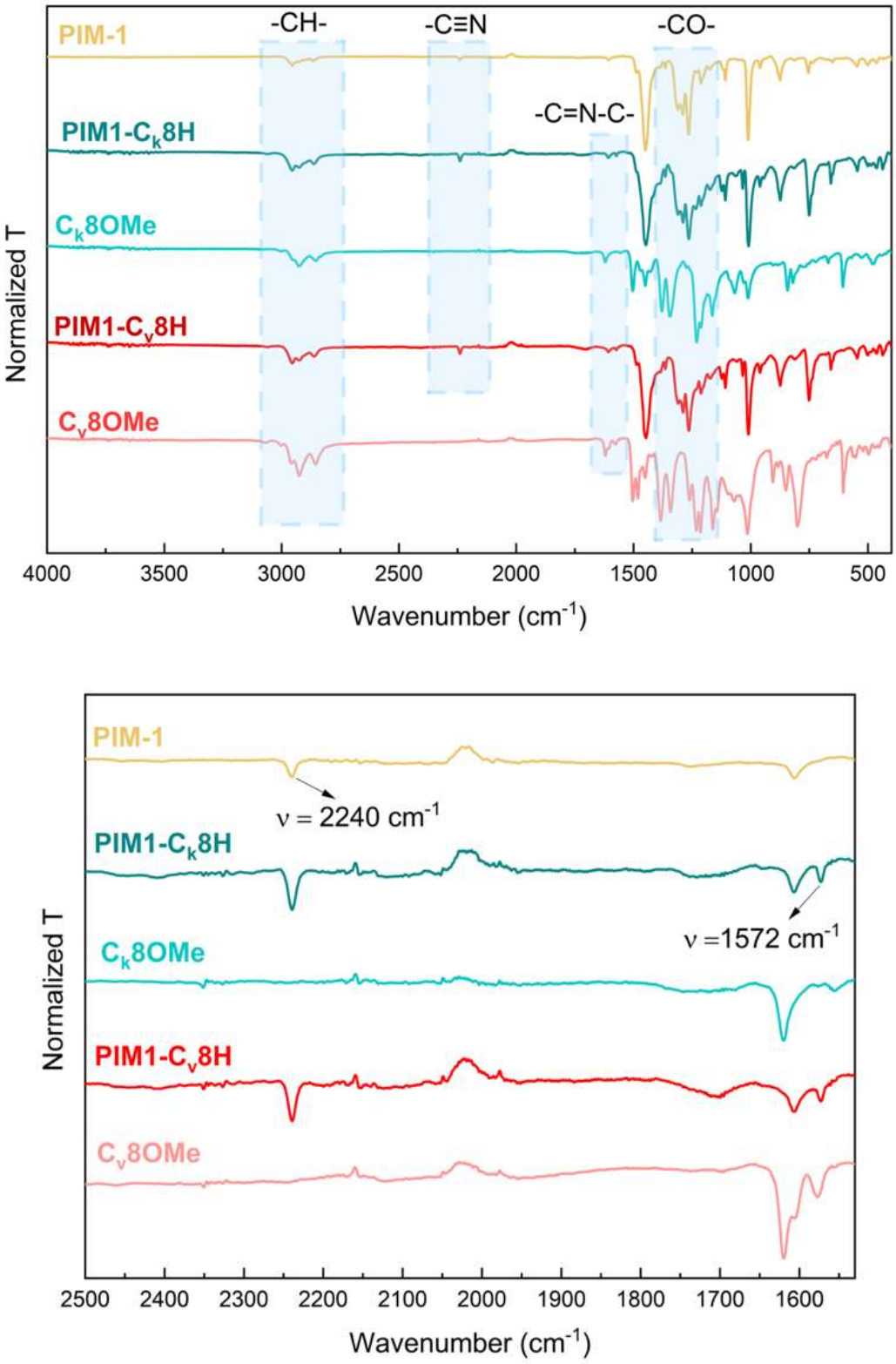

Figure S7. FT-IR full spectra (top) and zoom from 2500 to 1500 cm^{-1} (bottom) of **PIM1-C_V8H** and **PIM1-C_K8H** in comparison to the spectra of **C_V8OMe**, **C_K8OMe** and **PIM1**.

3. XPS Analyses

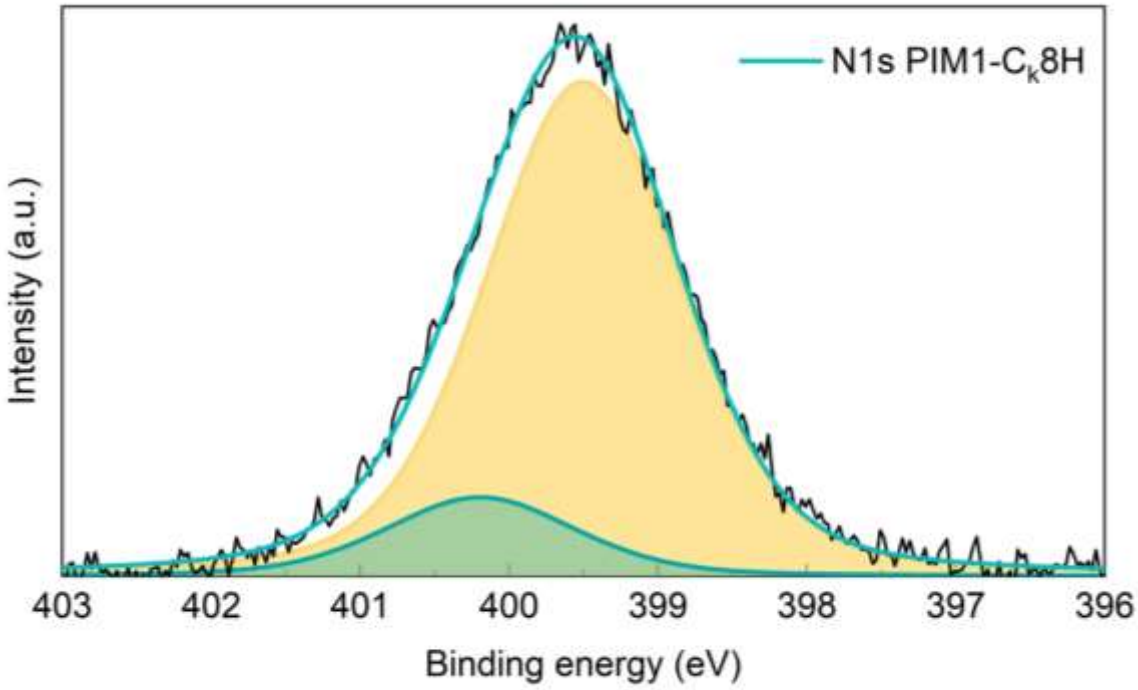

Figure S8. N1s core levels of **PIM1-C$_K$8H**.

The N1s photoemission signal must be normalized by the number of emitting nitrogen atoms for a proper quantification. Considering that homogeneous **PIM1-C$_V$8H** polymeric units *P* are analyzed, the N1s signal of **C$_V$8H** originated by 8 *P* nitrogen atoms. At the same time, **PIM1** signal derives from 2 n *P* nitrogen atoms, where n is the number of **PIM1** units (yellow part in Figure 2a) for each cavitand. Thus, the intensity ratio between the two peaks is (see XPS analyses section in S.I.):

$$n = 4 \cdot \frac{Int_{PIM1}}{Int_{CAV}} \quad (1)$$

The maximum error for n is about ±10%, mainly due to the uncertainty for the weak quinoxaline C=N-C component area. Thus, we conclude that the crosslinked **PIM1-C$_V$8H** and **PIM1-C$_K$8H** have about 38 and 26 **PIM1** units for each cavitand respectively (**Table S1**), i.e., about 9 and 6 monomers for each "wing", provided that the polymer structure is homogenous in the analyzed film.

Table S1. Number of PIM1 monomers for each cavitand calculated from the N1s core level analysis for the two crosslinked polymers.

	Exp. Int$_{PIM}$/Int$_{CAV}$	***n*, PIM monomers (±10%)**
PIM1-C$_v$8H	9.5	38.1±4
PIM1-C$_k$8H	6.5	25.9±3

4. TGA Analyses

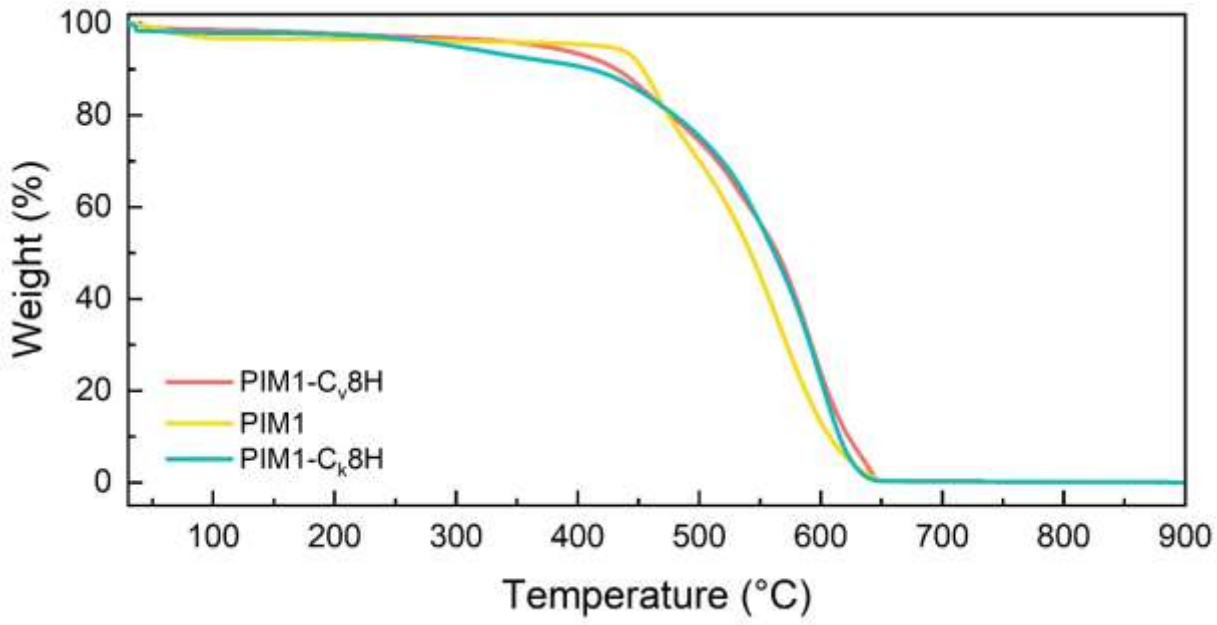

Figure S9. TGA curves of **PIM1**, **PIM1-C_V8H** and **PIM1-C_K8H**.

TGA analyses were performed in a temperature range of 30-900°C in air, with a heating rate of 10°C min^{-1}.

5. Blend fabrication

5.1. Preparation of the auxetic blends

PIM1, **PIM1-C_V8H** and **PIM1-C_K8H** were used for the preparation of the blend (**B0.1-C_V8H**, **B0.4-C_V8H, B0.8-C_V8H, B1.2-C_V8H**, **B1.2-C_K8H**) in different weight (**Table S2)**. Each blend weights 1.3 g and was obtained in a Petri dish of 9 cm ∅.

Table S2. Quantity of **PIM1**, **PIM1-C_V8H** and **PIM1-C_K8H** used for each blend.

	PIM1 (g)	**Crosslinked polymer (g)**
B0.1- C_V8H	1.287	0.013
B0.4-C_V8H	1.235	0.065
B0.8-C_V8H	1.170	0.130
B1.2-C_V8H	1.105	0.195
B1.2-C_K8H	1.170	0.130

General procedure for auxetic blend preparation

PIM1 was dissolved in chloroform and stirred overnight at room temperature. In a separated flask, a dispersion of **PIM1-C_V8H** (or **PIM1-C_K8H** for **B1.2-C_k8H** preparation), in chloroform was prepared and stirred overnight at room temperature. The two samples were mixed, vigorously stirred for 3 hours and then sonicated using an ultrasonic homogenizer (Hielscher UP200Ht, 200 W, 26 KHz) for 20 minutes. The dispersion was casted in a Petri dish (9 cm ∅), kept in a closed environment under a gently flow of nitrogen to allow the slow evaporation of the solvent over 48-72 hours. The dried film was then removed by detaching it carefully. The films obtained are reported in Figure S10.

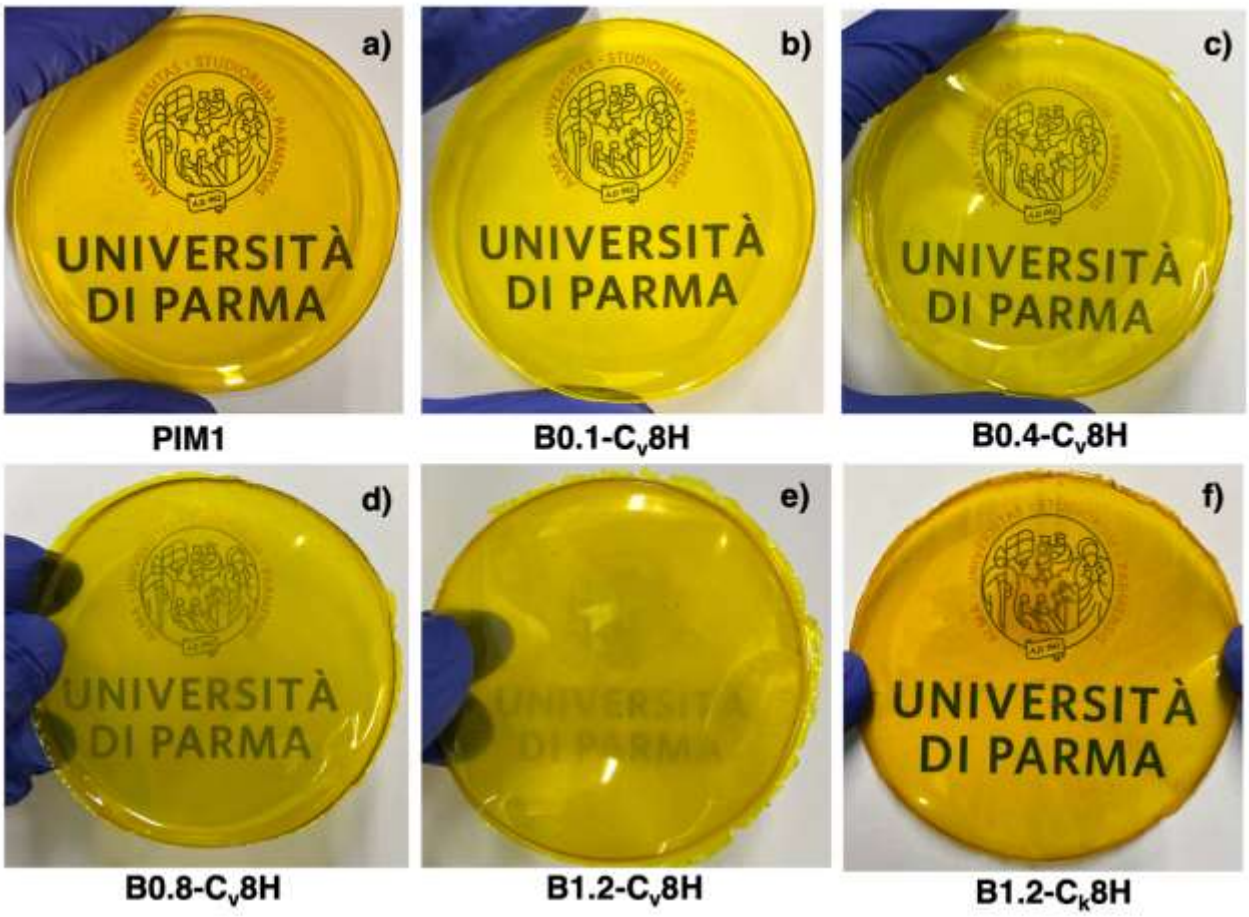

Figure S10. Photographs of: a) **PIM1** film, b-e) blends prepared *via* blending approach containing different portions of **PIM1-C$_V$8H.** It is visible, increasing the amount of crosslinked fraction in the blend, more defects appear in the film, thus resulting in opacity trend, f) blend with **PIM1-C$_K$8H**.

6. SEM Analyses

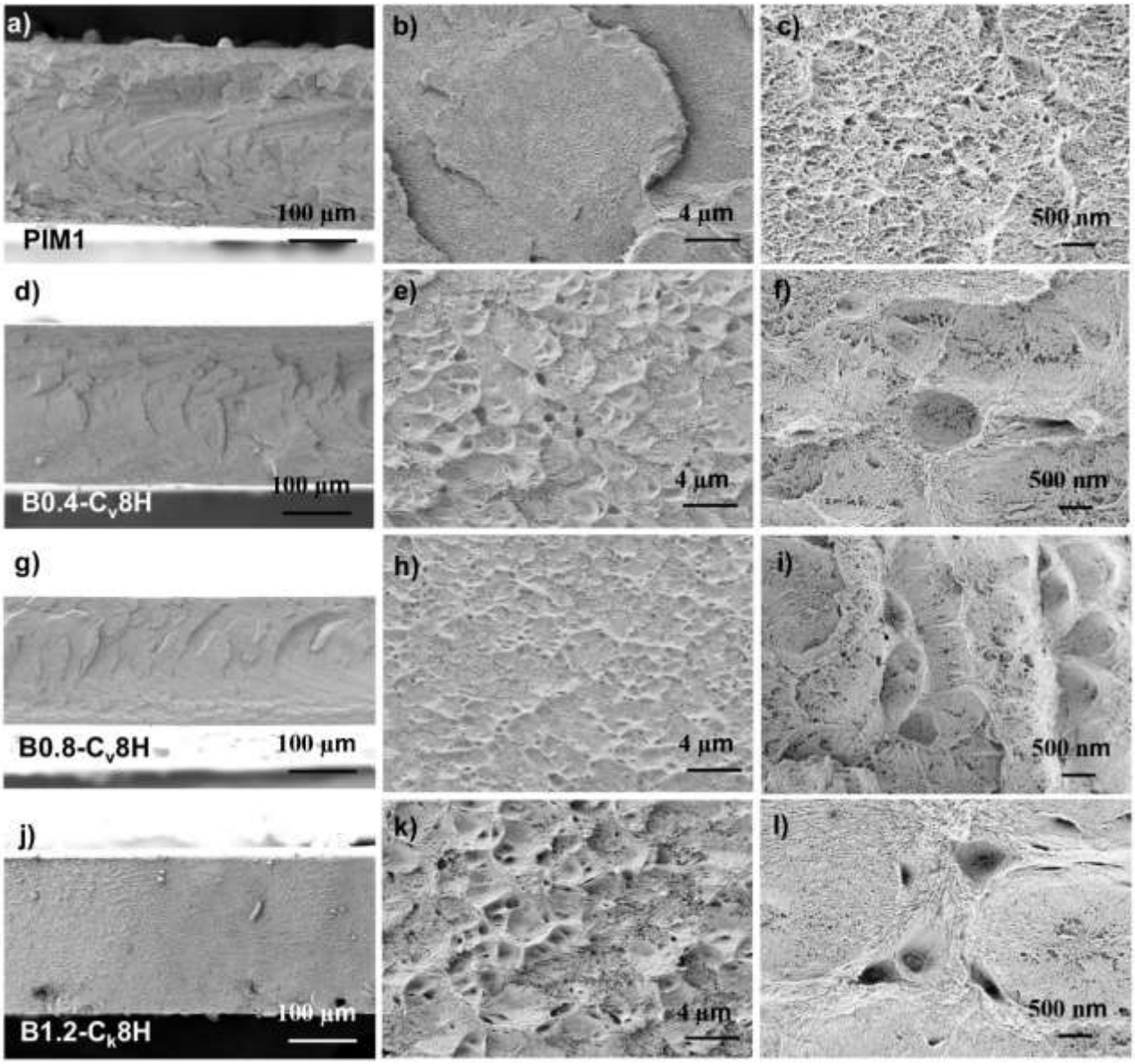

Figure S11. SEM cross section images and magnification images of **PIM1** (a, b, c), **B0.4-C$_V$8H** (d, e, f), **B0.8-C$_V$8H** (g, h, i), **B1.2-C$_K$8H** (j, k, l).

B0.1-C$_V$8H was not analyzed at SEM since it has not shown NPR, while **B1.2-C$_V$8H** exhibits an anomalous NPR trend, see Figure S13.

7. Mechanical tests

Mechanical tests were performed using a universal testing machine Galdabini® Quasar 2.5 on rectangular specimens having the size 50x10x0.2 mm. A tensile stretch has been applied to the specimens at a constant deformation rate equal to $\dot{\lambda_x} = 5 \cdot 10^{-4}\ s^{-1}$ until the maximum deformation was reached.

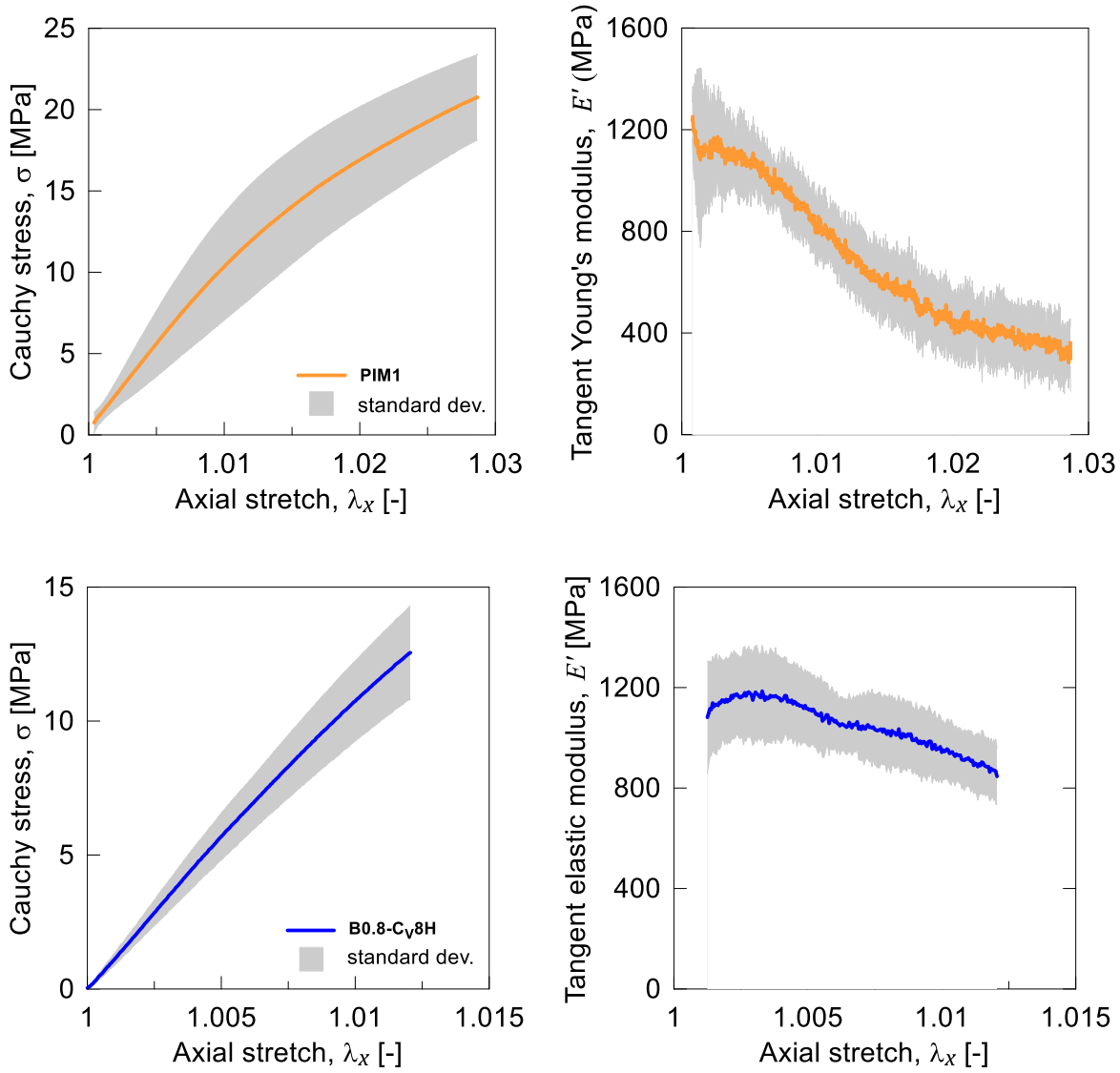

Figure S12. True Cauchy stress (left) and tangent elastic modulus (right) vs stretch for the standard **PIM1** (top) and for **B0.8-C$_V$8H** (bottom) specimens.

8. DIC analyses

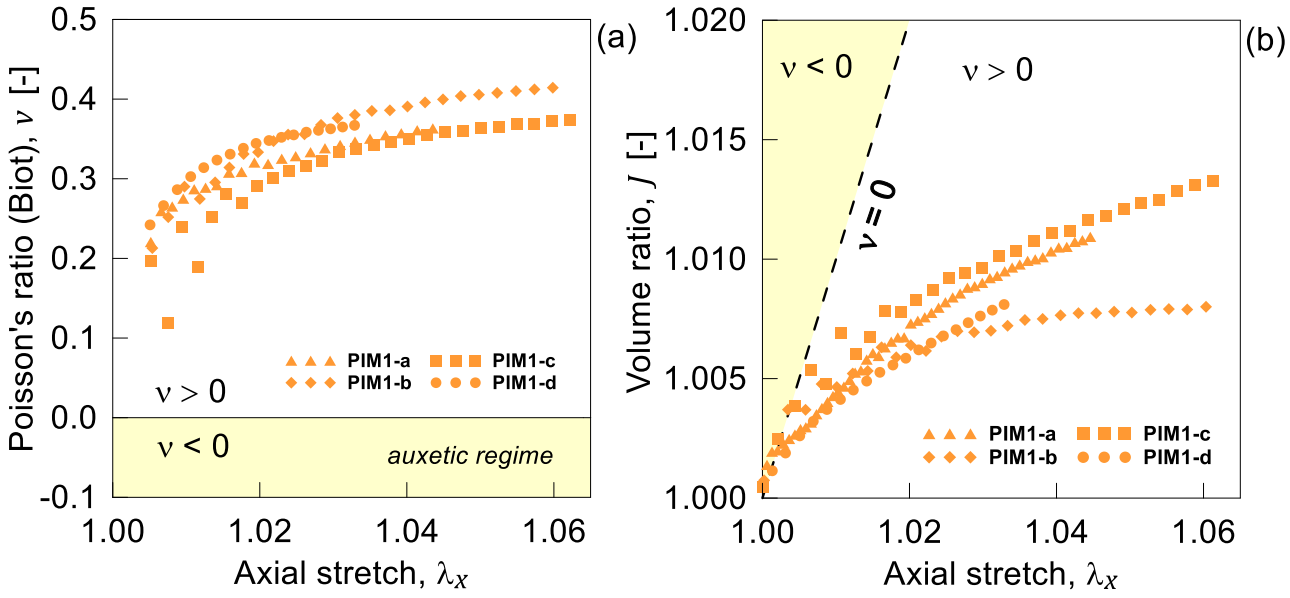

Figure S13. DIC analyses of **PIM1** specimens: (a): Average Poisson's ratio and (b) average volume ratio *vs* applied stretch λ_x.

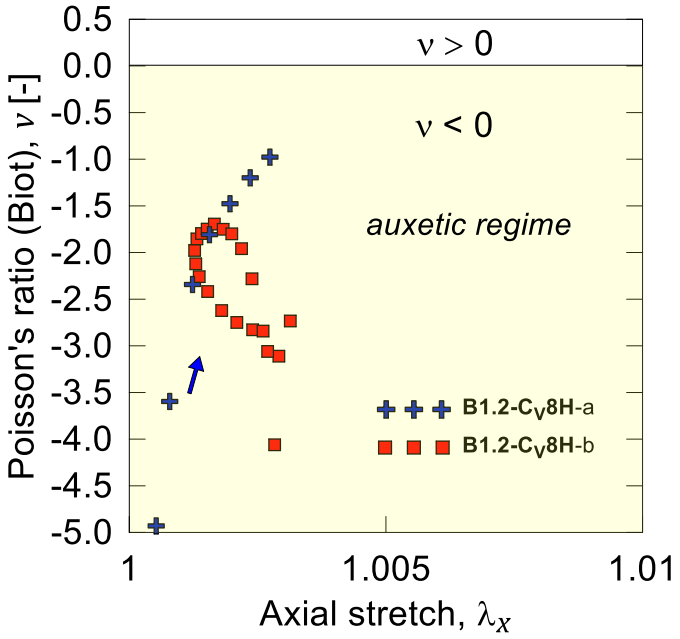

Figure S14. DIC analyses of **B1.2-C$_V$8H** on two different specimens showing irreproducible and anomalous NPR trend.

9. X-ray diffraction of PIM1 and B0.8-C_V8H films and powders

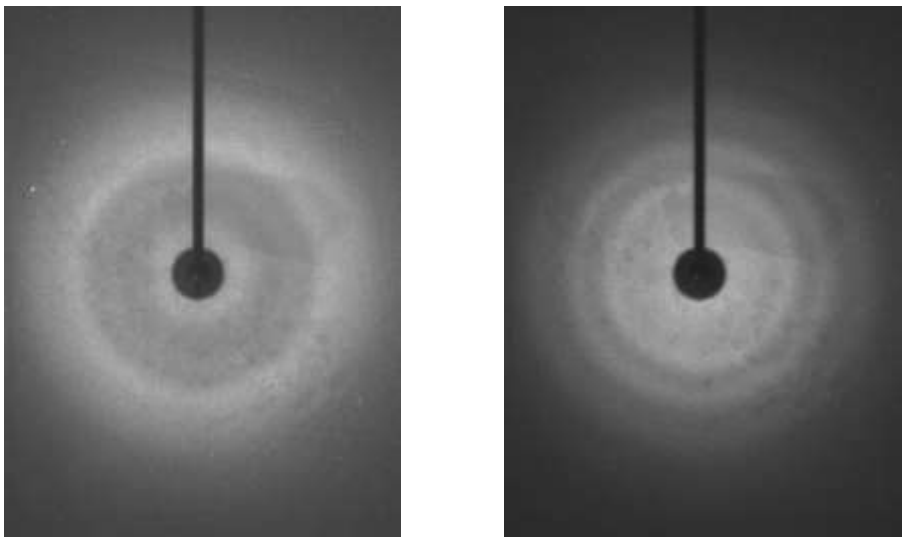

Figure S15. Diffraction patterns of **PIM1** (left) and **B0.8-C_V8H** (right) films with Cu K_a radiation.

Both films are fully amorphous and isotropic, as highlighted by the absence of diffraction figures in preferential directions. By comparison, also the X-ray powder diffraction of **PIM1** and **PIM1-C_V8H** are reported below, confirming that the starting material is also fully amorphous. The introduction of 8.0 % w/w of cavitand crosslinker in **PIM1** does not change the X-ray powder profile.

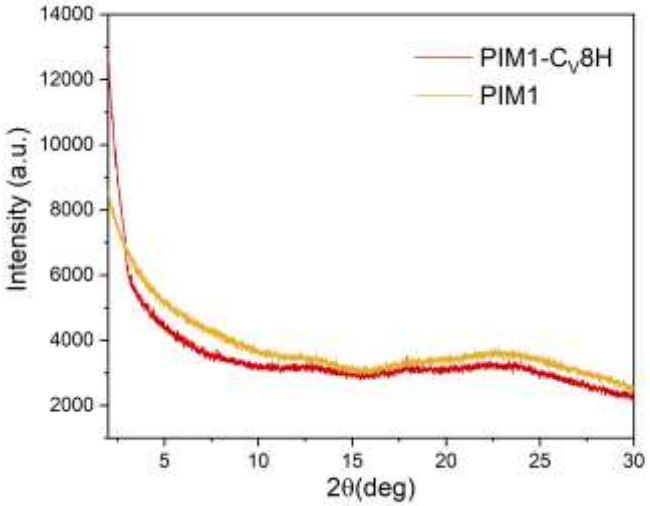

Figure S16. PXRD analysis of **PIM1** (orange trace) and **PIM1-C_V8H** (red trace).

10. Control films preparation

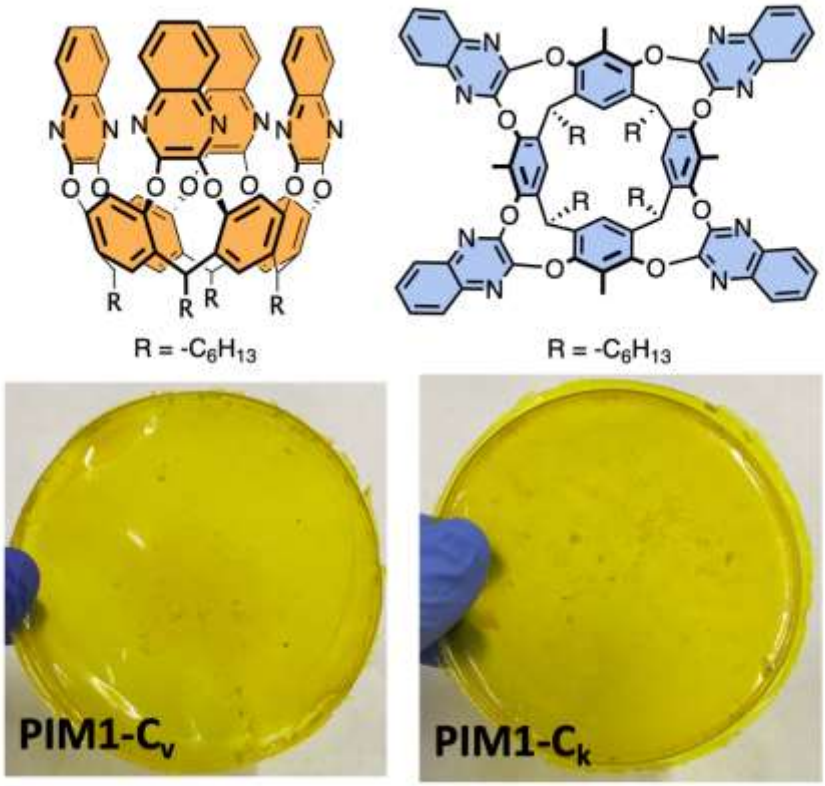

Figure S17. Chemical structure of $\mathbf{C_V}$ and $\mathbf{C_K}$ (top) dispersed in **PIM1** control film (bottom).

PIM1 (1.287 g) was dissolved in chloroform (30 mL), then $\mathbf{C_V}$ (13 mg) was added. The solution was stirred overnight at room temperature and casted in a Petri dish (9 cm ∅), and the solvent was allowed to evaporate in a closed compartment under a gentle nitrogen flow over 3 days. The same procedure and quantity were followed for the preparation of control film with $\mathbf{C_K}$. The obtained final films are shown in Figure S13.

$\mathbf{C_V}$ and $\mathbf{C_K}$ and their corresponsive resorcinarenes scaffold were prepared according to procedures reported in literature.[2][3]

11. Micromechanical theoretical model

The average mechanical properties of the proposed auxetic polymer can be estimated by knowing the cavitands volume fraction, the statistical parameters of the cavitand spatial distribution, and its geometric conformation change entity.

The mechanical properties of the PIM with cross-linked cavitand molecules are assessed by assuming that the smallest material volume element, referred to as the Representative Volume Element (R.V.E.)[4] (**Figure S18a**), correctly represents the average mechanical properties of the overall material having the same composition and microstructure of the R.V.E.

According to the Freely Jointed Chain (FJC) model, each polymer chain is modeled as a sequence of N rigid segments with length b[5], whose 3D arrangement is typically assumed to obey to the random walk theory[6]: the vector lying between the initial and final point of the chain is denoted by $\boldsymbol{r}$ (end-to-end vector). According to the rubber elasticity theory, the mechanical state of the material depends only on the distribution of the chains end-to-end vectors. Such a distribution is usually assumed to be Gaussian (**Figure S18b**).[7] By stretching the material, the initial distribution f_0 (corresponding to the stress-free state) changes due to the elongation of the chains lying along the loading direction and the contraction of the chains perpendicular to it (**Figure S18c**).

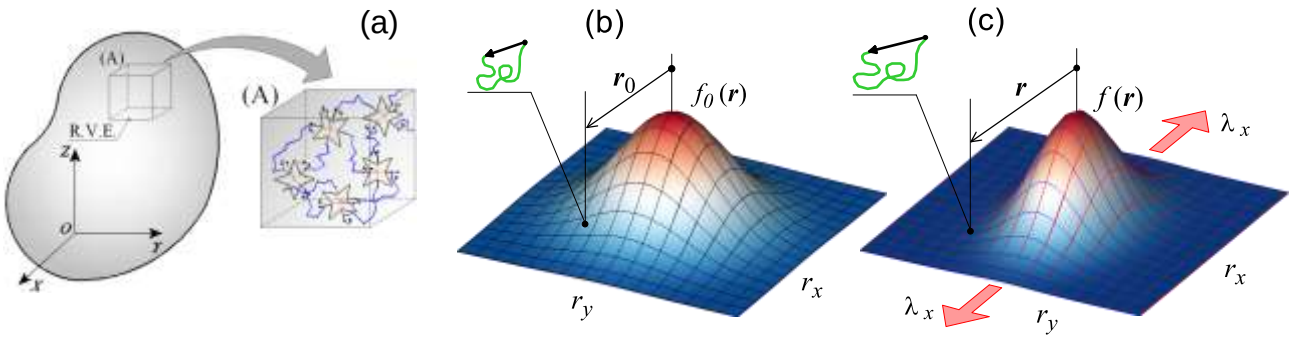

Figure S18. Schematic of the Representative Volume Element (R.V.E.) of a polymeric material containing auxeton elements (a). Schematic of the polymer's chains end-to-end distance distribution $f_0(\boldsymbol{r})$, $\boldsymbol{r} = (r_x, r_y)$ in a 2D chain network arrangement in the undeformed (b) and in a generic deformed (c) configuration.

The mechanical energy density of the material is evaluated as the difference between the energy density in the current (deformed) and in the initial (undeformed) state:

$$\Delta\Psi(t) = c_a\langle(f - f_0)\psi\rangle - p[J - (1 + \phi\, h\, J_{v\to k})] \qquad (2)$$

In Eq. (2) $\langle \dots \rangle$ indicates the integration over the chain configuration space, ψ is the mechanical energy per single chain, p is the hydrostatic pressure and $(1 + \phi\, h\, J_{V-K})$ is the volume change ratio due to the opening of the fraction $(\phi\, h)$ of cavitands, while c_a is the cross-link density. $J_{V-K} = V_k/V_v > 1$ (the subscripts K and V refer to the kite and vase configuration, respectively) indicates

the volume ratio related to the vase-kite conformation change, $0 \leq h \leq 1$ is the fraction of the open ones, ϕ is the total volume fraction of cavitands present in the unit volume of polymer.

Such an energy depends only on the current (deformed state, described by $f(\mathbf{r})$) and on the initial (undeformed state, described by $f_0(\mathbf{r})$) polymer's chains configurations, and provides the mechanical state of the material.[8] The dynamic nature of the equilibrium state of the cavitand opening mechanism obeys a balance reaction law, analytically described by the standard kinetic Eq. (3)[9]:

$$\frac{d\phi_k}{dt} = k_A\,\phi_v - k_D\,\phi_k \tag{3}$$

where $\phi = \phi_K + \phi_V$ is the total volume fraction of the cavitands, $\phi_K = h\,\phi$ and $\phi_V = (1-h)\phi$ are the volume fractions of the open (kite conformation) and close (vase conformation) molecules, while k_A, k_D are the activation and deactivation reaction rates, respectively.

Since the volume fraction of open molecules depends on the mechanical deformation of the network, we can write $\phi_K = h(\boldsymbol{F})\,\phi$, $\boldsymbol{F}$ being the deformation gradient tensor; Eq. (3) can be simply rewritten in term of h as follows:

$$\dot{h} = k_A - (k_A + k_D)h \tag{4}$$

where the time derivative has been indicated as $\dot{\blacksquare} = d\blacksquare/dt$.

The activation and deactivation rates, k_A, k_D, are functions of the energy barriers ΔG_{A0}, ΔG_{D0} existing between the two stable conformation states of the cavitand molecule when no external actions are applied (**Figure S19**); typically, they are expressed through the Arrhenius equation as follows

$$k_{A0} = C_A\,\exp\left(-\frac{\Delta G_{A0}}{k_B T}\right), \qquad k_{D0} = C_D\,\exp\left(-\frac{\Delta G_{D0}}{k_B T}\right) \tag{5}$$

where k_B, T are the Boltzmann constant and the absolute temperature, respectively, while C_A, C_D are the so-called frequency factors.[9]

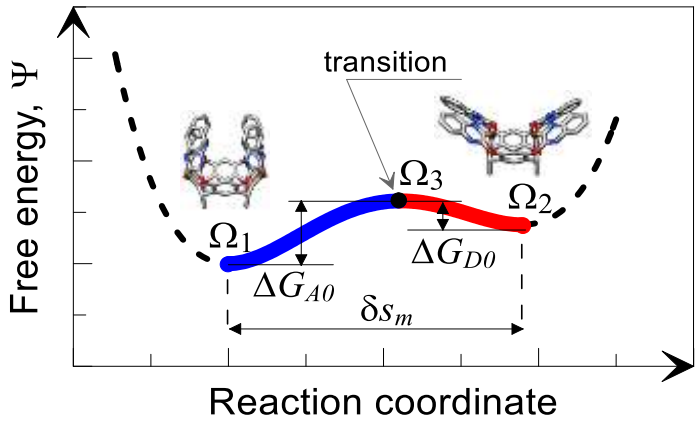

Figure S19. Schematic of the free energy vs reaction coordinate; the two stable configurations of the cavitand (vase and kite) are indicated with Ω_1 and Ω_2, respectively.

However, a mechanical force $\not{f}$ can affect the above-mentioned energy barriers, making the forward process (cavitand opening) favored and the backward one (cavitand closing) hindered.[10]

The increase of the forward and of the backward rates k_A, k_D, quantified with respect to their values in the unstressed state, k_{A0}, k_{D0}), can be expressed through the Arrhenius relationship as:

$$k_A = k_{A0}\ \exp\left(\frac{\not{f}\ \delta s_m}{k_B\ T}\right), \quad k_D = k_{D0}\ \exp\left(-\frac{\not{f}\ \delta s_m}{k_B\ T}\right) \tag{6}$$

being δs_m the size change of the molecule taking place between the close and the open state.[10][11]

11.1. Theoretical prediction of the Poisson's ratio

It is well-known that the Poisson's ratio (PR) of a material is defined only in the small deformation regime[12]; in the large deformation regime, the volume ratio $J = \det \boldsymbol{F}$ can be more conveniently adopted to quantify the volume change. A standard rubber usually has $\nu_0 \cong 0.5$ and, correspondingly, $J = 1$ because of its incompressibility (only isochoric deformations are possible); in other words, the volume ratio $J = V/V_0$ is constantly equal to 1 if the material cannot withstand volume variations. When a material is stretched along a given direction (say direction x) by an amount λ_x, it happens to be $J = \lambda_x$ when $\nu = 0$, while $J > \lambda_x$ when $\nu < 0$, i.e. for an auxetic material the volume ratio is greater than the amount of the applied stretch.

In absence of any constraint, by applying the stretch λ_x the stretches $\lambda_y = \lambda_z$ arise in the material normal to the stretch direction. According to the Biot definition, the Poisson's coefficient *vs* the applied stretch λ_x is given by[12]:

$$\nu_{xy}(\lambda_x) = \nu_{xz}(\lambda_x) = \nu(\lambda_x) = -\frac{\lambda_y - 1}{\lambda_x - 1} = -\frac{\lambda_z - 1}{\lambda_x - 1} \tag{7}$$

and results to be variable with the deformation. The Poisson's ratio becomes equal to the nominal PR ν_0, which is a characteristic value for any given material when the deformation tends toward zero, in the limit of no stretch applied, i.e. for $\lambda_x \to 1$. In other words, the standard or nominal Poisson's coefficient ν_0 is a material characteristic only for small deformations, while for large stretches it must be evaluated by using Eq. (7). According to our experimental measurements, the Poisson's ratio of the standard **PIM1** is equal to about $\nu_0 \cong 0.38$.

A simple micromechanical model to assess the Poisson's coefficient in PIM containing cavitand molecules can be defined according to the mechanism taking place at the chain network scale.

When the polymeric network is crosslinked to the cavitand molecules, their conformation change affects the deformation arising in the material; in this case, the above Eq. (7) has to be modified as follows:

$$\nu(\lambda_x) = -\frac{\lambda_{yt}-1}{\lambda_x-1} = -\frac{\lambda_{zt}-1}{\lambda_x-1} \tag{8}$$

where the total stretches λ_{yt}, λ_{zt} account for both the mechanical deformation and the deformation induced by the cavitand expansion effect.

We assume that the cavitand conformation change takes place at a critical microscopic stretch $\bar{\lambda}$ according to the following activation function $0 \leq h(\lambda_x) \leq 1$:

$$h(\lambda_x) = \frac{\exp\frac{(\lambda_x-\bar{\lambda})}{c}}{1+\exp\frac{(\lambda_x-\bar{\lambda})}{c}} \tag{9}$$

where $\bar{\lambda}$, c are a model parameters to be determined by fitting experimental data. In other words, the fraction of open cavitand molecules is zero if $\lambda_x \ll \bar{\lambda}$, it is $h = ½$ if $\lambda_x = \bar{\lambda}$, while $h(\lambda_x) \to 1$ when $\lambda_x \gg \bar{\lambda}$, while c defines the steepness with the applied deformation of the amount of cavitands switching from the vase to the kite state. When a uniaxial stretch λ_x is applied to a material whose Poisson's coefficient is ν, its volume ratio is expressed as:

$$J = \lambda_x - 2\nu(1+\lambda_x) \tag{10}$$

As mentioned above, when microscopic deformations arise in the material such as in the case of cavitand molecules switching from the vase to the kite state, such a mechanism has to be considered through the use of the total stretches in order to correctly evaluate the volume change.

Upon opening of all the cavitands (whose volume fraction is ϕ) contained in the generic volume V of material, the volume ratio of the polymer becomes:

$$J_n = \frac{V(1-\phi)+\phi V J_{V-K}}{V} = 1+\phi(J_{V-K}-1) \tag{11}$$

In the above expression, $J_{V-K} = 2.62$ represents the volume ratio of a single cavitand molecule, i.e. the ratio between the final and the initial volume of a single molecule (see **Figure 1b**). By considering – on the basis of the above described synthesis procedure – that the cavitand molecules are homogeneously and isotropically distributed in the polymer network, the above-mentioned volume increase induces the following stretches in the polymer:

$$\lambda_{yc} = \lambda_{zc} = 1+\phi\, h(\lambda_x)(\lambda_c-1) \tag{12}$$

where we have assumed the material to be mechanically stretched along the x-direction. The average cavitand stretch due to its vase→kite conformation change can be evaluated as $\lambda_c = J_n^{1/3}$.

Finally, the total value of the stretches arising in the material due to the combination of the externally applied stretch λ_x and to the cavitand opening are:

$$\lambda_{yt} = \lambda_y + (\lambda_c - 1), \quad \lambda_{zt} = \lambda_z + (\lambda_c - 1) \tag{13}$$

According to the above-described micromechanical model, upon opening of the cavitand molecules the Poisson's ratio starts from the nominal value $\nu_0 \cong 0.38$ and, by increasing the stretch, it rapidly decreases, reaching negative values (auxetic behavior).

When all cavitands are already open (the fraction of the molecules in the vase conformation among all the cavitand molecules present in the unit volume is $h(\lambda_x) = 1$), the cavitand opening mechanism does not provide any further microscopic expansion to the material; by further increasing the applied stretch, the Poisson's ratio tends to reach that of the standard polymer without cavitand molecules (Eq. (7)). This happens because, for sufficiently high applied stretch values, the network deformation is not affected any more by the already completed cavitand expansion.

As can be observed from Eq. (9) and **Figure 1**, the earlier the cavitand begin to open (small values of $\bar{\lambda}$) the more auxetic is the material.

12. Poisson's ratio determination

A so-called region of interest (ROI) have been defined in the reference initial image (prior to the test, undeformed configuration) of the specimens; the dots within such a ROI have been automatically tracked by the DIC software across all the images recorder during the mechanical tests in order to determine the deformation map along the x- and y-directions. Finally, as mentioned above, a post processor software[13] was used to extract the deformations along user defined lines (virtual extensometers, see continuous and dotted lines in **Figure 3b**); 6 virtual extensometers ($1x$, $2x$, …, $6x$) have been set in the x-direction and 12 ($1y$, $2y$, …, $12y$) in the y-direction of the ROI. The evaluation of the Poisson's ratio has been obtained by using Eq. (8) by employing the average value of the deformations provided by the virtual extensometers placed in the Cartesian $x-y$ directions, namely $\bar{\varepsilon}_{xt}$, $\bar{\varepsilon}_{yt}$, respectively. The Poisson's ratio, expressed as a function of the applied stretch λ_x, is finally determined as follows:

$$\nu(\lambda_x) = -\frac{(1+\bar{\varepsilon}_{yt})-1}{(1+\bar{\varepsilon}_{xt})-1} = -\frac{\bar{\varepsilon}_{yt}}{\bar{\varepsilon}_{xt}} \tag{14}$$

where the expressions $\bar{\lambda}_{xt} = 1 + \bar{\varepsilon}_{xt}$, $\bar{\lambda}_{yt} = 1 + \bar{\varepsilon}_{yt}$ have been used to evaluate the total average stretches arising in the material.

13. Reversibility of the auxetic behavior upon repeated cycling tests

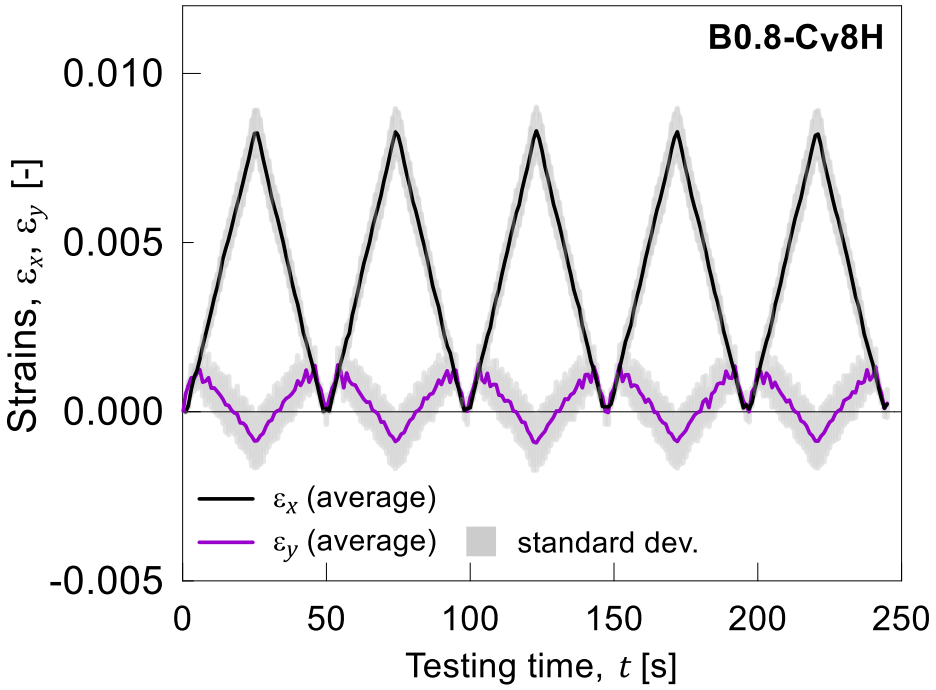

Figure S20. Average strain $\varepsilon_y = \lambda_y - 1$ determined from experimental tests *vs* the applied stretch $\varepsilon_x = \lambda_x - 1$. **B0.8-Cv8H** subjected to five stretch cycles. It can be noted that under an applied tensile (positive) deformation ε_x the transversal deformation ε_y is is positive (expansion). The reversibility of the deformation is clearly visible, being the two deformation cycles almost identical. The standard deviation shown in the figure is evaluated by using the measurements provided by the virtual extensometers of the DIC analysis (6 in x-direction and 12 in y-direction, see Fig. 3b) placed on a single specimen.

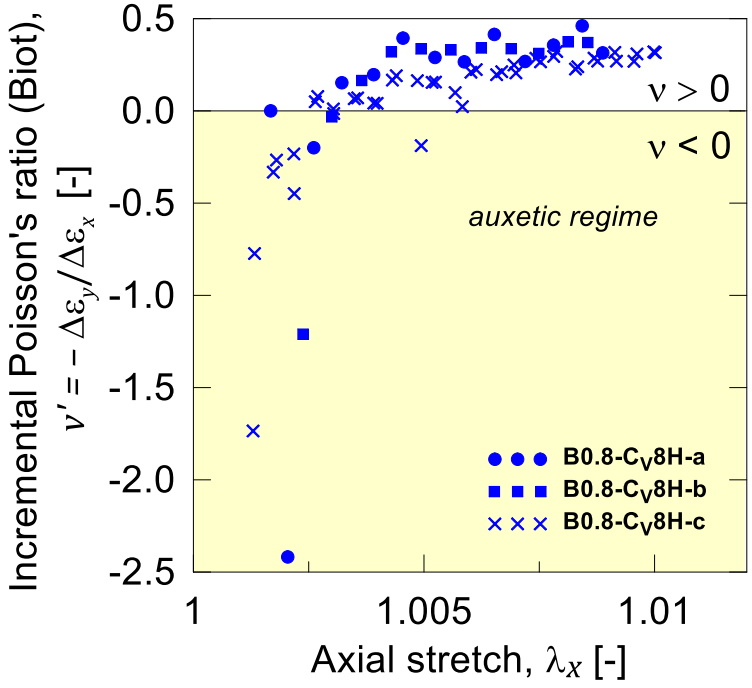

Figure S21. Trend of the incremental PR vs the applied stretch for **B0.8-Cv8H** specimens

14. References

[1] P. M. Budd, E. S. Elabas, B. S. Ghanem, S. Makhseed, N. B. McKeown, K. J. Msayib, C. E. Tattershall, D. Wang, *Adv. Mater.* **2004**, *16*, 456.

[2] J. R. Moran, J. L. Ericson, E. Dalcanale, J. A. Bryant, C. B. Knobler, D. J. Cram, *J. Am. Chem. Soc.* **1991**, *113*, 5707.

[3] L. M. Tunstad, J. A. Tucker, E. Dalcanale, J. Weiser, J. A. Bryant, J. C. Sherman, R. C. Helgeson, C. B. Knobler, D. J. Cram, *J. Org. Chem.* **1989**, *54*, 1305.

[4] S. Nemat-Nasser, M. Hori, J. D. Achenbach, *Micromechanics: Overall Properties of Heterogeneous Materials*, Elsevier Science, Amsterdam, **2014**.

[5] W. Kuhn, F. Grün, *Kolloid-Zeitschrift* **1942**, *101*, 248.

[6] E. Helfand, *J. Chem. Phys.* **1975**, *62*, 999.

[7] F. J. Vernerey, R. Long, R. Brighenti, *J. Mech. Phys. Sol.* **2017**, *107*, 1.

[8] E. M. Arruda, M. C. Boyce, *J. Mech. Phys. Sol.* **1993**, *41*, 389.

[9] P. Hänggi, P. Talkner, M. Borkovec, *Rev. Mod. Phys.* **1990**, *62*, 251.

[10] H. A. Kramers, *Physica* **1940**, *7*, 284.

[11] R. Brighenti, F. Artoni, F. Vernerey, M. Torelli, A. Pedrini, I. Domenichelli, E. Dalcanale, *J. Mech. Phys. Sol.* **2018**, *113*, 65.

[12] M. F. Beatty, D. O. Stalnaker, *J. Appl. Mech.* **1986**, *53*, 807.

[13] Ncorr_post: DIC Post-Processing Tool, open source 2D digital image correlation MATLAB post processor, http://mech.fsv.cvut.cz/~nezerka/DIC/downloads.htm (last access on 26th Apr. 2023).